Responses and Explanations on new the revision

(From the author of the manuscript egusphere-2025-5393, Qimeng Li)

16 March 2026

To Reviewer 2

We gratefully acknowledge the reviewer 2 for the careful review of our manuscript and for providing detailed and valuable comments. We believe that these comments have significantly contributed to improving the scientific quality and presentation of the manuscript. We have addressed all comments point by point, and the corresponding revisions have been incorporated into the revised version.

1) The authors use multiple datasets and discuss different variables, in the manuscript some of the instrumentation, methodology and uncertainties are described, but there is a lack of information on others, like PM2.5, PM10 and meteorological and radiometric measurements at the surface level. This is worthy information to be included, bearing in mind some of the correlation analyses included in the manuscript.

Reply: We thank the reviewer for pointing out this important issue. We agree that, given the correlation analyses presented in the manuscript, a comprehensive description of the surface measurements is essential.

In the revised manuscript, Section 2 has been substantially expanded to include:

"PM_{10} and $PM_{2.5}$ concentrations were measured using β-ray absorption particulate matter monitors (LGH-01B and LGH-01E). Both instruments operate over a concentration range of 0−1000 μg m^{-3}, with a minimum sampling interval of 30 min and a sampling flow rate of 16.7 L min^{-1}. The lower detection limit is < 2 μg m^{-3}, and the flow stability is within 2 %. Surface meteorological variables were obtained from an automatic weather station (DZZ5). Atmospheric pressure is measured over a range of 500–1100 hPa with a resolution of 0.1 hPa and a maximum permissible error of ±0.3 hPa. Air temperature is measured over a range of −50 to 50 °C, with a resolution of 0.1 °C and a maximum permissible error of ±0.2 °C. Relative humidity is measured over 5–100 %, with a resolution of 1 %, and maximum permissible errors of ±3 % for RH ≤ 80 % and ±5 % for RH > 80 %.Surface solar irradiance was measured using a TBQ-2-UMB pyranometer, which has a spectral response range of 0.3–3 μm and a measurement range of 0–2000 W m^{-2}. The hourly measurement uncertainty is approximately 8 %."

2) Section 2.2 must be improved with the inclusion of some graphical information on the study area.

Reply: Thank you very much for this valuable suggestion. We fully agree with the reviewer's comment and have added a map of the study area in Section 2.2. The geographical information of the study area is now shown in Fig. 1.

The updated figure is shown below.

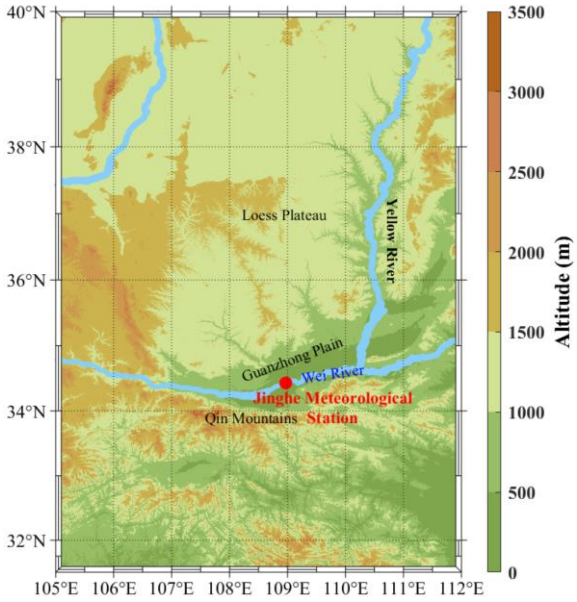

Figure 1. Geographical coverage around observation site (31°30′–40°N, 105°–112°E). The red dot indicates the location of the Jinghe National Meteorological Station in Xi'an (34°26′N, 108°58′E).

3) Given the relevance of the temperature and relative humidity profiling and the accessibility of the reference Li et al. 2025, additional details on the associated methodology must be included in the manuscript for helping the reader understand better the pros and cons of these retrievals. I realized that the authors provided yet an answer to this question through the answer they gave to the Reviewer#1 review. But concerning the new figure 1, and the explanation offered in the answer to the Reviewer #1, I do not understand the small size of the shaded area associated to the corrected temperature profile in red, having in mind the uncertainty associated to the cross talk correction method, evidenced in the new figure 1g, where it is necessary to include information on the regression coefficient and the standard error of the modelled cross-talk.

Reply: We thank the reviewer for this detailed and technically important comment. Because the absolute error of the uncorrected temperature is relatively large, displaying the full absolute error of the uncorrected temperature (grey shading) would reduce the visibility of the corrected temperature absolute error (red shading). We fully agree with your suggestion and have therefore added a linear regression analysis between the cross-talk–corrected temperature profile and the radiosonde temperature profile in Fig. 1. The regression coefficients and standard deviation information are also provided to improve transparency. The cross-talk regression yielded $R^2 \approx 0.799$ (n=372, ≤1.5 km), with a residual standard error of 0.366 K.

Changes in manuscript:

The atmospheric temperature correction technique is based on establishing a linear relationship between the backscatter ratio and the elastic-scattering crosstalk ratio, which allows the rotational Raman ratio to be corrected using the measured backscatter ratio. Figure 2 illustrates the temperature retrieval process based on this algorithm. First, a high-altitude region unaffected by the geometric overlap factor is selected, and radiosonde temperature profiles are used for system calibration. Under clear-sky and dry near-surface conditions, the theoretical rotational Raman ratio is derived

from radiosonde data (black dash–dotted line in Fig. 2a). By comparing it with the measured Raman ratio (blue solid line in Fig. 2a), the geometric overlap factor is obtained (red solid line in Fig. 2b), enabling overlap correction. Next, the theoretical Raman ratio under strong elastic-scattering conditions is derived from radiosonde data (black dash–dotted line in Fig. 2d). The measured Raman ratio (black solid line in Fig. 2d) is then used to calculate the elastic-scattering crosstalk ratio. A linear regression between the backscatter ratio and the crosstalk ratio is performed to determine the system calibration constant (Fig. 2e). Using this constant together with the measured backscatter ratio, the rotational Raman ratio is corrected, enabling retrieval of the atmospheric temperature profile within the elastic-scattering region (Fig. 2f). A linear regression between the corrected lidar temperature and the radiosonde temperature yields a coefficient of determination (R^2) of approximately 0.8 (Fig. 2g), indicating good agreement between the two measurements. A detailed description of the algorithm can be found in Li et al. (2025).

The updated figure is shown below.

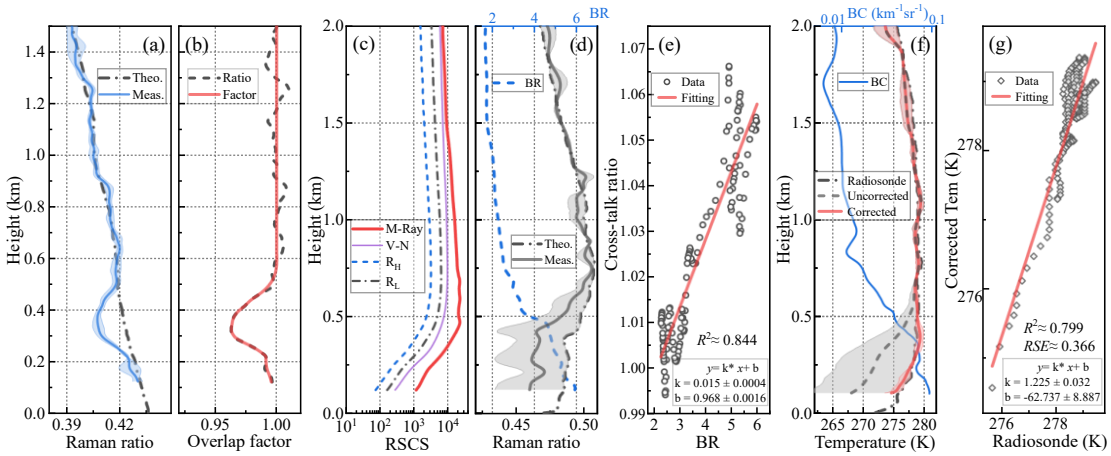

Figure 2. Atmospheric temperature correction. (a) Measured (blue solid) and theoretical (black dash–dotted) rotational Raman ratios. (b) Overlap-related quantities, including the measured ratio (black dashed) and the overlap function (red solid). (c) Range-square-corrected signals from the elastic (Mie–Rayleigh; thick red solid), nitrogen vibrational Raman (thin purple solid), and high- and low-quantum-number rotational Raman (black dash–dotted and blue dashed) channels. (d) Backscatter ratio (blue dash–dotted) and rotational Raman ratios (measured ratio, black solid; theoretical ratio, black dash–dotted). (e) Linear regression between the backscatter ratio (BR) and the cross-talk ratio. (f) Backscatter coefficient (BC) and temperature profiles derived from lidar measurements and radiosonde observations. The black dash–dotted line denotes the radiosonde temperature, while the red solid and blue dashed lines represent the corrected and uncorrected lidar temperature profiles, respectively. Shaded areas indicate the corresponding uncertainties. (g) Linear regression between radiosonde and lidar temperatures.

4) The discussion on figure 7 is not easy to follow, the redesign of this figure could help to solve this problem. In general, the sizes of figures could be larger to clearly detect the significant features of the situation. Likely shortening the number of time slots presented and improving the visibility of the most relevant periods. Identifications of the upper aerosol layer and the top of the TI in the profiles of figure 7 could improve the discussion.

Reply: We thank the reviewer for the constructive comments. Figure 7 in the original manuscript (now Figure 8 in the revised version) is primarily intended to illustrate the day-to-day evolution of the vertical structures of aerosols and temperature during the pollution development stage. To facilitate comparison between the vertical structures of aerosols and temperature, we have redesigned Fig. 7 following your suggestion. Specifically, the font size of the text and numerical labels in the figure has been increased to improve the visualization of the key information.In addition,

we focus on the vertical structure distributions in the morning and evening to highlight the characteristic features during these important periods more clearly. The upper boundary of the aerosol layer and the top of the temperature inversion have been specifically marked in the figure.

The updated figure is shown below.

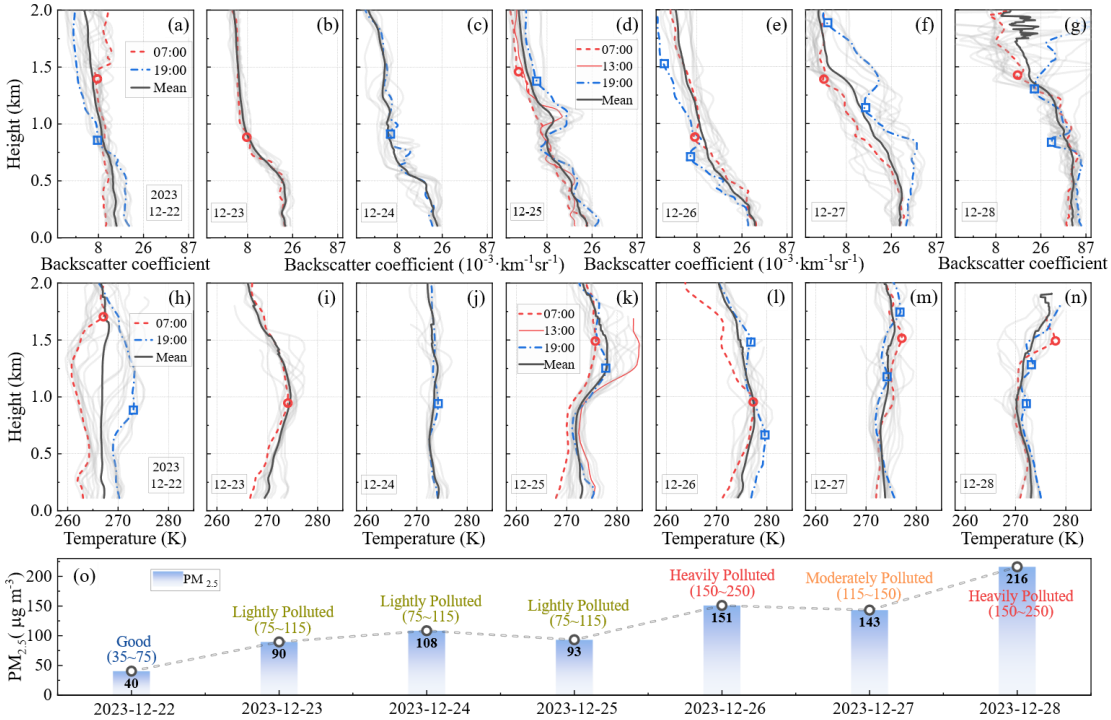

Figure 8. Vertical profiles of aerosol backscatter coefficient and temperature from 22 to 28 December. Panels (a)–(g) show the aerosol backscatter coefficient profiles. The red dashed and blue dash–dotted lines denote the profiles at 07:00 and 19:00, respectively. The black solid line represents the daily mean profile, while the grey solid lines indicate hourly profiles. Red circles and blue squares mark the upper boundary of the aerosol layer in the morning and evening, respectively. Panels (h)–(n) show the temperature profiles with the same plotting conventions. Red circles and blue squares indicate the top heights of the temperature inversion in the morning and evening, respectively. Panel (o) shows the daily mean $PM_{2.5}$ concentration.

We carefully checked the entire manuscript and found that the font size in Fig. 2 (now Figure 3 in the revised version) also required adjustment. Therefore, the figure has been redrawn to improve its visual clarity, as shown below.

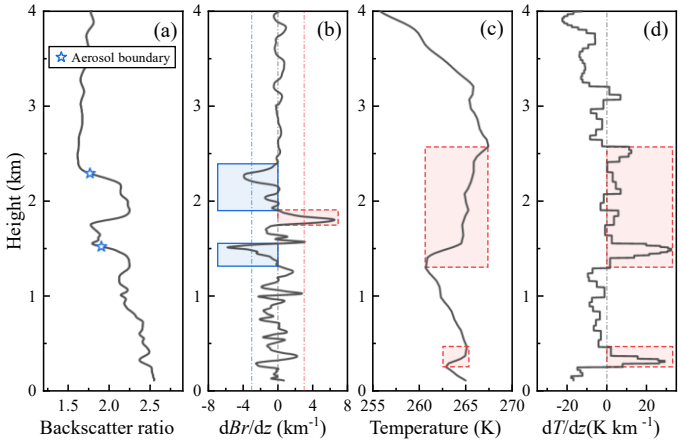

Figure 3. Extraction of UABL and TI characteristics. Panels (a)-(d) show (a) BR, (b) BR gradient, (c) temperature, and (d) temperature gradient. In panels (a)-(d), the black curves represent the BR, BR gradient, temperature, and temperature gradient, respectively. Asterisks indicate the identified aerosol layer boundaries. In panel (b), the blue

solid and red dashed shaded regions denote NIBR and PIBR, respectively. In panels (c) and (d), the red dashed shaded regions highlight the TI layers.

5) Even with the information gathered with the comprehensive set of observations use in this study some statements are a little bit speculative. For example, in line 221, the authors write:" A brief removal of pollutants occurred in the afternoon of 30 December, followed by a rapid re-accumulation during the night.". In fact what you can state is that: "A brief reduction of pollutants occurred in the afternoon of 30 December, followed by a rapid re-accumulation during the night." The origin of the "reduction" could be associated to different causes like the removal, the spreading of these pollutants in a high volume of atmosphere and the advection of these pollutants due to horizontal wind, but the authors do not present evidence for a choice.

Reply: We thank the reviewer for this insightful comment. We agree that the original wording may imply a specific mechanism for pollutant removal that is not fully supported by the available observations. To avoid potential overinterpretation, we have revised the wording in the manuscript following the reviewer's suggestion. Specifically, the phrase "removal of pollutants" has been replaced with "reduction of pollutants" to provide a more cautious description of the observed change in $PM_{2.5}$ concentration.

The sentence in the manuscript has therefore been revised as follows:
"A brief reduction of pollutants occurred in the afternoon of 30 December, followed by a rapid re-accumulation during the night."

This modification avoids attributing the reduction to a specific mechanism. In addition, we have carefully reviewed the entire manuscript and revised several statements to ensure that the interpretations remain closely supported by the observations and to avoid potential overinterpretation.

The following text shows the revisions to the description:

"A brief reduction of pollutants occurred in the afternoon of 30 December, followed by a rapid re-accumulation during the night."

"The lidar and radiosonde temperature profiles indicate that a surface-based TI layer with a thickness of up to 600 m developed in the morning of 30 December, effectively suppressing the vertical diffusion of aerosols. Consequently, despite strong north-westerly winds exceeding 8 m s^{-1} above approximately 1 km during the daytime (Fig. 6h), surface $PM_{2.5}$ concentrations remained persistently high (Fig. 4a). As surface heating intensified, the associated decrease in relative humidity may have promoted aerosol drying and enhanced turbulent mixing in the lower atmosphere, leading to a noticeable reduction in near-surface $PM_{2.5}$ concentrations. However, the duration of surface heating was relatively short, potentially limiting the sustained development of turbulence and thereby restricting efficient vertical transport of aerosols. Later in the day, $PM_{2.5}$ concentrations increased again, possibly associated with aerosol subsidence and hygroscopic growth."

"The top height of the surface-based temperature inversion decreased from approximately 0.7 km at 10:00 to about 0.4 km at 13:00. Meanwhile, the near-surface aerosol backscatter coefficient showed an overall decreasing trend. A pronounced gradient in the backscatter profile corresponded well with the inversion top height. Considering the relatively high near-surface

relative humidity (up to 80 %) during this period, the observed decrease in backscatter is likely dominated by aerosol drying in the lower layer, possibly accompanied by moderate aerosol radiative forcing."

6) In their answers to the Reviewer#1, the authors try to improve the discussion on the stove effect starting in line 305: "... At noon on 24 December, aerosols were primarily concentrated near the surface, potentially favoring the onset of the stove effect. However, the surface-based TI restricted vertical diffusion, resulting in negligible changes in surface PM2.5 concentrations." and in this sense they propose the inclusion of a new statement : "However, the warming of the lower layer must overcome the surface inversion formed by nocturnal radiative cooling, which delays the development of near-surface turbulence and may be the primary reason for the relatively modest changes in surface PM2.5 concentrations." My concern with this justification is that I can see in the figures a clear effect of surface inversion, that supports this statement. Even with the answer on the overlap effects on temperature offered by the authors, determining the presence of near surface temperature inversion is not easy, having in mind the uncertainties in the temperature profiles in the lower part and the fact that you missed the first 120 m, according to the estimation of the overlap.

Reply: Thank you for raising this important point. Due to the limitations associated with the overlap correction, reliable temperature retrieval in this study begins at approximately 120 m above the surface. Consequently, the complete structure of the surface-based temperature inversion cannot be fully resolved by the lidar observations. The "near-surface temperature inversion" described in the manuscript therefore refers only to the temperature structure above the reliable retrieval height, rather than the classical surface-based inversion layer.

Although the temperature structure in the lowest layer can be inferred to some extent using radiosonde observations, we have added a clarification at the first occurrence of the term "near-surface inversion" in the manuscript to ensure a more rigorous description:

"It should be noted that the description of the surface-based TI layer here refers only to the region above the reliable temperature retrieval height (>120 m)."

Regarding the interpretation mentioned in the manuscript, our analysis was also supported by radiosonde temperature profiles. As shown in Fig. 5f, the radiosonde observation at 07:00 on 24 December indicates the presence of an inversion in the lowest layer. We apologize for not stating this clearly in the previous version. Accordingly, the relevant sentence in the manuscript has been revised as follows:

"However, the radiosonde temperature profile on the morning of 24 December (Fig. 5f) indicates the presence of a near-surface inversion, which may delay surface warming and the development of turbulence in the lower atmosphere and could partly explain the relatively small variation in surface $PM_{2.5}$ concentration."

7) Having in mind the relevance of the stove effect in the discussion of results, does the author measurements of the absorption component of the aerosol, for example with an aethalometer, that can support the development of the stove effect near the surface.

Reply: We thank the reviewer for this valuable suggestion. Unfortunately, direct measurements

of aerosol absorption (e.g., from an aethalometer) were not available during this experiment. To provide indirect evidence, we followed the reviewer's suggestion and calculated the lidar ratio. Since the lidar ratio is influenced by aerosol absorption and scattering properties, it can provide indirect support for the interpretation of the stove effect near the surface.

Nevertheless, it should be noted that this inference is based on optical properties derived from lidar observations and has not been directly verified by dedicated aerosol absorption measurements.

8) In the manuscript the authors mention the extinction coefficient as a product of their measurements, but they do not use this variable. In fact, the lidar ratio that can be derived from the backscatter and extinction profiles could provide confirmation of the absorption component of the aerosol relevant for the development of the dome effect.

Reply: We thank the reviewer for this constructive suggestion. Following this comment, we further analyzed the extinction coefficient and derived the corresponding lidar ratio at 355 nm ($S = \alpha/\beta$) to better characterize the aerosol optical properties. The updated results are presented in the revised Fig. 10(d), together with the aerosol heating rate shown in Fig. 10(c).

The lidar ratio exhibits a clear vertical variation. In the near-surface layer (below ~300 m), the lidar ratio ranges from approximately 60–80 sr, while at around 1 km altitude it mainly remains within 35–50 sr. According to previous studies, lidar ratios above 60 sr at 355 nm are typically associated with strongly absorbing urban or pollution aerosols. Therefore, the elevated lidar ratio observed near the surface suggests enhanced aerosol absorption in the lower layer.

Consistent with this feature, the aerosol heating rate (Fig. 10c) also shows pronounced positive values primarily confined to the near-surface layer, indicating stronger radiative heating associated with the accumulation of absorbing aerosols. In contrast, the elevated aerosol layer around 1 km does not show similarly high lidar ratios or heating rates.

These results suggest that the strongest absorption and associated radiative heating are mainly confined to the lower aerosol layer. Consequently, the potential stove effect is more likely related to the accumulation of absorbing aerosols near the surface rather than to an elevated absorbing layer. The manuscript has been revised accordingly to clarify this point.

The updated figure is shown below.

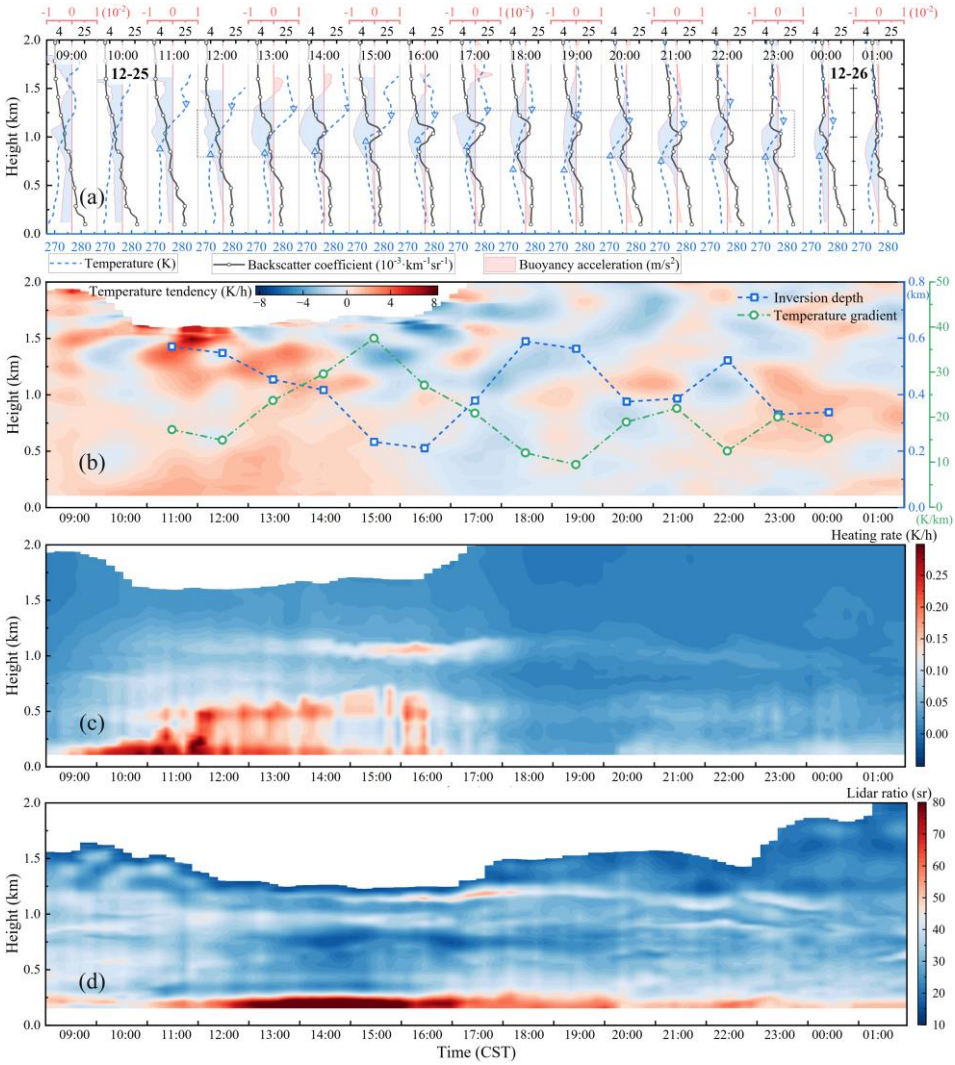

Figure 9. Evolution of the vertical structure and atmospheric buoyancy on 25 December. Panels (a)–(d) show the aerosol and temperature structure, buoyancy acceleration, aerosol heating rate, and lidar ratio (355 nm), respectively. In panel (a), the black line with circle markers represents the aerosol backscatter coefficient, and the blue dashed line denotes the temperature profile. Shading represents buoyancy acceleration, with blue (red) corresponding to negative (positive) values and downward (upward) buoyant motion. Upward- and downward-pointing triangles indicate the temperature inversion (TI) layer. In panel (b), the green dotted line shows the temperature gradient, while the blue dash–dotted line with square markers represents the TI depth.